International Journal of Engineering

Journal Homepage: www.ije.ir

Nonlinear Control for Positive Output Super Lift Luo Converter in Stand Alone Photovoltaic System

S. A. A Fallahzadeh[a], N. R Abjadi*[a], A. Kargar[a], F. Blaabjerg[b]

[a] *Faculty of Engineering, Shahrekord University, Shahrekord, Iran*
[b] *Department of Energy Technology, Aalborg University, Aalborg, Denmark*

PAPER INFO

Paper history:
Received 27 September 2019
Received in revised form 27 October 2019
Accepted 16 Januray 2020

Keywords:
Photovoltaic
Sliding Mode Controller
Stand Alone
Super Lift Luo converter

ABSTRACT

This paper proposes a stand-alone photovoltaic (PV) system based on a DC-DC positive output super lift Luo (POSLL) converter. A conventional sliding mode control, a sliding mode controller using a simple sign function and a linear controller using proportional integrator (PI) are used for the control of the PV panel voltage and POSLL converter inductor current and these methods are compared together. The POSLL converter is a DC-DC converter with higher voltage gain compared to other conventional DC-DC converters, and has a good voltage regulation with a simple structure. The stability and accessibility of the proposed nonlinear controls are investigated widely. The internal dynamics of the proposed closed-loop control systems are also investiged. A practical implementation of the system on a hardware setup is performed using a low cost Discovery real time digital control platform. The experimental and simulation results demonstrate the validity of the proposed control schemes over a stand-alone real photovoltaic system.

***doi**: 10.5829/ije.2020.33.02b.08*

1. INTRODUCTION

In recent years, with the increased use of renewable energy sources, photovoltaic (PV) generator systems have an inevitable effect on generation of electricity [1, 2]. In PV applications, several topologies are used to interface the PV generator with the grid or load. These are applied through power electronic devices such as DC-DC converters and DC-AC inverters. PV systems can work in isolated mode or grid-connected mode. The advantages of using the photovoltaic in generating electricity include the avoidance of pollutants emissions, silent operation, long lifetime and low maintenance requirement. Moreover, solar energy is abundant, free, clean and inexhaustible. When the connection of PV energy to the grid is infeasible or expensive, for example, in some remote areas, the stand-alone PV systems can be considered. Therefore, many PV systems operate in stand-alone mode, such a system consists of a PV generator, energy storage (for example a battery), DC to AC converters, AC and DC consumers and a power conditioning system [3].

DC-DC step-up converters are used in many electronic devices. The main requirements for these converters are to provide a large conversion ratio, high power density and high efficiency. Recently, more interests are devoted to DC-DC converters called Luo converters [4-5]. This is because of their universality and relative simplicity. One of the most interesting converters in the family of Luo converters is positive output super-lift Luo (POSLL) converter [6–9]. In fact, these converters consist of three types of converters: elementary circuit, re-lift circuit, and triple-lift circuit. Voltage gain and switching gain of POSLL DC-DC converter is more than other conventional converters like Boost, Cuk, Buck, Z-source converters. Also, the average of the inductor current in POSLL converter is less than those converters. So it can be used at higher powers. Moreover, the existence of an additional capacitor in its circuit causes the output voltage ripple be more reduced. Therefore,

*Corresponding Author Email: *navidabjadi@yahoo.com* (N. R.Abjadi)

Please cite this article as: S.A.A Fallahzadeh, N.R Abjadi, A. Kargar, F. Blaabjerg, Nonlinear Control for Positive Output Super Lift Luo Converter in Stand Alone Photovoltaic System, International Journal of Engineering (IJE), IJE TRANSACTIONS B: Applications Vol. 33, No. 2, (February 2020) 237-247

a DC-DC POSLL converter is used to increase the voltage level of PV panel with a relatively higher voltage gain and a lower inductor current compared to a conventional Boost converter.

To control the desired objectives of PV systems, linear controllers are commonly used. The linear controllers are very useful to serve their purposes over a fixed set of operating points as these controllers are mainly designed based on linearized models of the PV systems. For this reason, linear controllers are unable to achieve desired control objectives under a wide variation of operating points, i.e., under fast changing of weather conditions and reference value. Nonlinear controllers are used to overcome the drawback of operating points for PV systems. In literature, there are different types of nonlinear controllers of PV systems such as Sliding Mode Controller (SMC), Feed- Back Linearizing (FBL) controller, and backstepping controller. In [9], a nonlinear controller based on passivity analysis is proposed for regulating the output voltage of a DC-DC boost power converter in a stand-alone PV system; however the proposed control is not robust and one should control the input voltage to achieve the maximum power point tracking (MPPT) from PV pannel. The sliding mode control technique offers several advantages compared to traditional control methods: stability, even for large line and load variations, robustness, good dynamic response and simple implementation. In [10], using a boost converter in a PV system again the output voltage is controlled which is not suitable for MPPT porpuses, moreover, the stabilty of internal dynamic was not investigated. In [11], a robust backstepping controller is desined for a buck boost converter in a PV system which has a complicated structure. In [12], an adaptive fuzzy sliding mode control is designed for a boost converter in a PV system; using fuzzy conrtol, there is no gauranty for overal system stability and the process of design is complicted. In [13], a backstepping sliding controller is designed for a boost converter which controlls the input voltage; however, the proposed sliding varible depends to system parameters and the robustness of SMC is lost.

In this paper, considering the merrits of POSLL converter compared to conventional converters, the control of a stand-alone PV system consisting of a POSLL converter is investigated. Three different controllers: proportional–integral (PI) controller, sign function sliding mode controller (SFSMC) and conventional sliding mode controller (CSMC) are used and compared. The detailed discussion on the existence and stability conditions of the CSMC and SF-SMC for POSLL converter are studied. The contributions of the paper are as follows: the state space equations of the proposed PV system are obtained using a model degree reduction to simplify the control design; two sliding mode controllers are designed for the PV+POSLL converter, and they are compared with conventional PI controllers. Considering sliding mode controllers, the attractiveness of the surfaces are presented and the stability of the internal dynamics are investigated and analyzed.

The behaviour of the POSLL converter in CCM has been analysed in Section 2. The voltage control based on PI, SFSMC and CSMC is presented in Section 3. Both simulation and experimental results are presented in Section 4. Finally, the conclusion is given in Section 5.

2. PV SYSTEM MODEL

The stand-alone PV system connected to a load is shown in Figure 1. The system consists of PV panel and input capacitor, DC-DC POSLL converter and the load.

Voltage Lift (VL) technique has been widely used in power electronics systems. It has provided a good way to solve the problem of the output voltage and power transfer efficiency of DC-DC converters limitations. Figure 2-a shows an elementary circuit of the proposed system using POSLL converter, and Figures 2-b 3-c show the equivalent circuits when switch S is on (closed) and switch S is off (open), respectively.

From Figure 2-b, it can be seen that the capacitor C_1 (v_{C_1}) is charged to the input voltage of the converter (V_{pv}) when switch *S* is on. Since inductor L_1 and capacitor C_1 are connected in parallel, the current of inductor L_1 (i_{L_1}) will increase. As shown in Figure 2-c, during switch-off, the voltage across inductor L_1 will become $-(V_o - 2V_{pv})$, hence i_{L_1} will decrease. The average of the inductor voltage is zero in steady state. It is assumed that *UT* is the period that switch is on and *(1-U)T* is the period that switch is off. As a result, the voltage gain (VG) of the POSLL converter is as follow:

$$VG = \frac{V_o}{V_{in}} = \frac{2-U}{1-U} \quad (1)$$

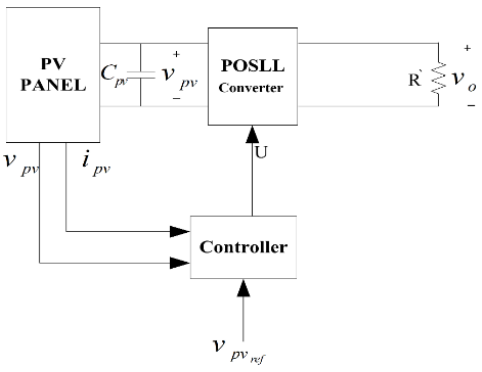

Figure 1. The configuration of the proposed system controller

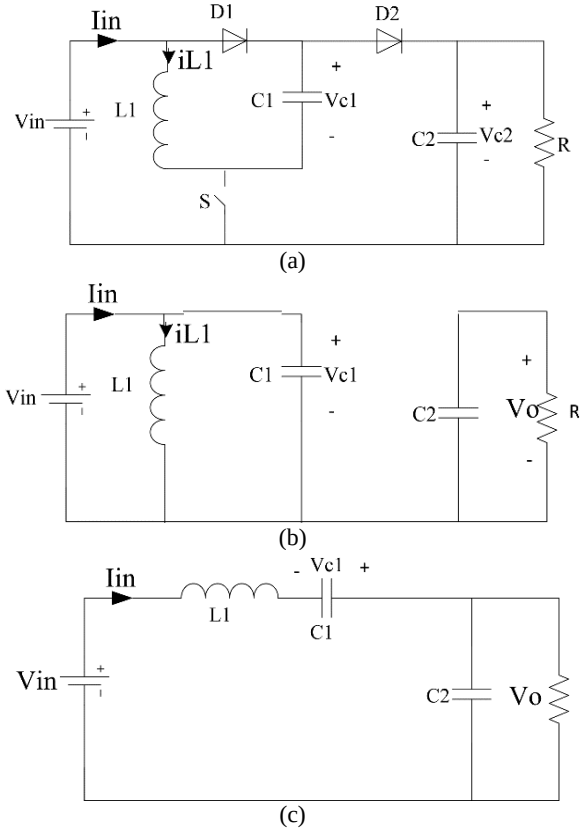

Figure 2. An **e**lementary circuit of the proposed system. (a) Elementary Circuit diagram. (b) Equivalent Circuit diagram when S switch is on. (c) Equivalent Circuit diagram when S switch is off

where U and V_O are the duty cycle of the power switch and output voltage of converter, respectively.

The capacitor voltage v_{C_1} is fixed with the assumption that the capacitor value C_1 is large enough. Therefore, the following relation is obtained for all times $v_{pv} = v_{c_1}$. As a result, the average model of the DC-DC POSLL converter is expressed as:

$$\begin{aligned} \dot{i}_{L_1} &= \frac{1}{L_1}((v_o - v_{pv})U + (2v_{pv} - v_o)) \\ \dot{v}_O &= \frac{1}{C_2}(i_{L_1} - \frac{v_O}{R} - i_{L_1}U) \\ \dot{v}_{pv} &= (\frac{i_{pv} - i_{L1}}{C1 + C_{pv}})U + \frac{(i_{pv} - i_{L1})(1-U)}{C_{pv}} \end{aligned} \quad (2)$$

where $U \in (0,1)$. The capacitor voltage v_{C_2} is fixed with the assumption that the capacitor value C_2 is large enough. Therefor, the state equations are obtained as:

$$\dot{z} = \begin{bmatrix} 0 & \frac{2}{L_1} \\ \frac{-1}{C_{pv}} & 0 \end{bmatrix} z + \begin{bmatrix} \frac{1}{L_1}(v_o - v_{pv}) \\ \frac{i_{pv} - i_{L1}}{C1 + C_{pv}} - \frac{(i_{pv} - i_{L1})}{C_{pv}} \end{bmatrix} u(t) + \begin{bmatrix} \frac{-v_o}{L_1} \\ \frac{i_{pv}}{C_{pv}} \end{bmatrix} \quad (3)$$

where

$$z = [i_{L_1} \; v_{pv}]^T, \dot{z} = [\dot{i}_{L_1} \; \dot{v}_{pv}]^T \quad (4)$$

The above equations can be written in the following canonical form

$$\dot{z} = f(z) + g(z)u(t) \quad (6)$$

where

$$f(z) = \begin{bmatrix} 0 & \frac{2}{L_1} \\ \frac{-1}{C_{pv}} & 0 \end{bmatrix} z + \begin{bmatrix} \frac{-v_{c_2}}{L_1} \\ \frac{i_{pv}}{C_{pv}} \end{bmatrix} = \begin{bmatrix} \frac{2v_{pv} - V_{C_2}}{L_1} \\ \frac{-i_{L_1} + i_{pv}}{C_{pv}} \end{bmatrix}$$
$$g(z) = \begin{bmatrix} \frac{1}{L_1}(v_{c_2} - v_{pv}) \\ \frac{i_{pv} - i_{L1}}{C1 + C_{pv}} - \frac{(i_{pv} - i_{L1})}{C_{pv}} \end{bmatrix} \quad (6)$$

3. CONTROL OF SYSTEM

Figure 1 shows the overall schematic diagram of a stand-alone PV system with the proposed controls. In this section, three controllers including PI, CSMC and SF-SMC are presented.

3. 1. DC-DC POSLL Converter In this section, the performance of linear control using two series PI controllers is presented. The reference value of the solar panel terminal voltage is determined by the MPPT algorithm and the control system is used to track the reference. Dual-loop control strategy is chosen for the POSLL converter, where the output of the outer voltage loop is set as the reference value for the inner current control loop which is shown in Figure 3. $K_1 \& K_2$ are gains of the PI controllers and $T_1 \& T_2$ are time constants of the PI controllers, in second.

3. 2. SMC Controller Using Sign Function (SF-SMC) The control objective is the convergence of the input voltage v_{pv} to a desired equilibrium value $v_{pv_{ref}}$. A direct control is an approach in which the output variable v_{pv} is used to synthesize a suitable sliding surface representing the desired objective. The alternative is then to use, as a sliding surface coordinate function, a function

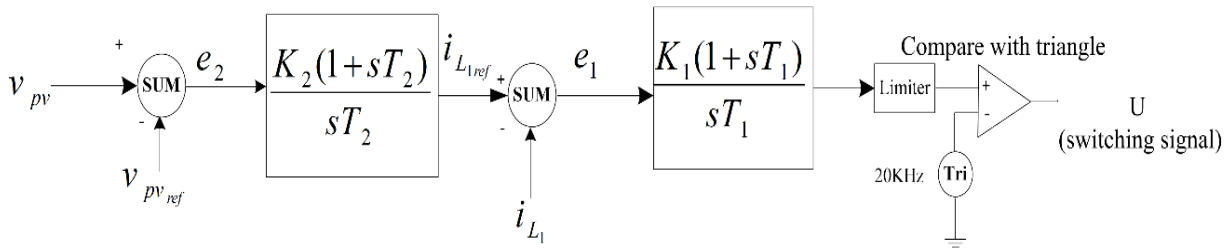

Figure 3. Schematic diagram of the proposed controller using PI

that, when set to zero, reproduces the desired equilibrium value of the input inductor current, in correspondence with the desired output equilibrium voltage, this method is known as indirect method.

3. 2. 1. Direct Controller Method a Direct control approach in which the output variable v_{pv} is used to synthesize a suitable sliding surface representing the desired objective is presented. In this method, the sliding variable is considered as:

$$s_1 = e(z,t) \quad where \quad e(z,t) = v_{pv} - v_{pv_{ref}} \tag{7}$$

Equating the derivative of the sliding variable to zero, the equivalent control is obtained as:

$$\begin{aligned} \dot{s}_1 &= \frac{\partial e(z,t)}{\partial z}\dot{z} = \frac{\partial e(z,t)}{\partial z}[f(z) + g(z)u_{eq}(z,t)] \\ &= L_f e(z,t) + L_g e(z,t)u_{eq}(z,t) \end{aligned} \tag{8a}$$

$$u_{eq}(z,t) = -\frac{L_f e(z,t)}{L_g e(z,t)} = \frac{c_{pv} + c_1}{c_1} \tag{8b}$$

where

$$\begin{aligned} L_f e(z,t) &= \frac{\partial e(z,t)}{\partial i_L} f_1(z,t) + \frac{\partial e(z,t)}{\partial v_{pv}} f_2(z,t) = \frac{i_{pv} - i_L}{c_{pv}} \\ L_g e(z,t) &= \frac{\partial e(z,t)}{\partial i_L} g_1(z,t) + \frac{\partial e(z,t)}{\partial v_{pv}} g_2(z,t) = \frac{i_{pv} - i_L}{c_{pv} + c_1} - \frac{i_{pv} - i_L}{c_{pv}} \end{aligned} \tag{9}$$

Considering necessary condition in (13) , this equivalent control is not possible because $u_{eq}(z,t) > 1$.

3. 2. 2. Indirect Controller Method Consider the following sliding variable for inductor current

$$e(z,t) = i_{L_1} - i_{L_{1ref}} \tag{10}$$

where $i_{L_{1ref}}$ is the reference value of i_{L_1} that is obtained from comparison of PV panel voltage v_{pv} and its reference $v_{pv_{ref}}$ using a proportional integrator (PI) controller. One can drives the output function $e(z,t)$ to zero by a discontinuous control which means that the inductor current coincides with the desired average equilibrium inductor current. Applying the Lie derivative theory:

$$\begin{aligned} L_f e(z,t) &= \frac{\partial e(z,t)}{\partial i_L} f_1(z,t) + \frac{\partial e(z,t)}{\partial v_{pv}} f_2(z,t) = \frac{2v_{pv} - v_o}{L} \\ L_g e(z,t) &= \frac{\partial e(z,t)}{\partial i_L} g_1(z,t) + \frac{\partial e(z,t)}{\partial v_{pv}} g_2(z,t) = \frac{-v_{pv} + v_o}{L} \end{aligned} \tag{11}$$

where f_1 and f_2 are the frist and second rows of $f(z,t)$ in Equation (8), repectively. Also g_1 and g_2 are the first and second rows of $g(z,t)$ in Equation (6), repectively. $L_f e(z,t)$ is the Lie derivative of $e(z,t)$ relative to $f(z,t)$. The equivalent control according to $\dot{e}(z,t) = \dot{i}_{L_1} = 0$ is obtained as:

$$u_{eq}(z,t) = -\frac{L_f e(z,t)}{L_g e(z,t)} = \frac{-2V_{pv} + V_o}{V_o - V_{pv}} \tag{12}$$

The ideal sliding dynamics occurs when $u_{eq}(z,t)$ acts on the system as a feedback function while the system is ideally satisfying the condition $e(z) = 0$. Let assume that $L_g e(z,t) > 0$ in a neighborhood of manifold $S = \{z \mid e(z,t) = 0\}$ (i.e., $L_g e(z,t)$ is strictly positive, "above" and "below" S in the vicinity of this surface), then $\dot{e}(z,t)$ should be strictly negative at the point z. So, one must choose the control that beats the positive incremental effect that this term has over the derivative of *e*. We must then let $u(z,t) = 0$. $\dot{e}(z,t)$ for this control input entirely coincides with $L_f e(z,t)$. It follows that being $L_g e(z,t) > 0$ in an open neighborhood of S, it is necessary that $L_f e(z,t)$ be strictly negative in a neighborhood of S.

Let now assume that the point z is located "below" the surface, i.e., $e(z,t) < 0$ then, it can be seen that for the trajectories to reach and cross the sliding manifold S, $\dot{e}(z,t)$ must be strictly positive. Since $L_g e(z,t) > 0$ and $L_f e(z,t) < 0$, one must choose $u(z,t) = 1$ so as to

magnify the positive incremental effect of $L_g e(z,t)$ over the time derivative of $e(z,t)$.

The necessary and sufficient condition for the local existence of a sliding state over the smooth manifold $S=\{z \mid e(z,t)=0\}$ is that the equivalent control satisfies:

$$0<u_{eq}(z,t)<1,\ z\in S \tag{13}$$

Since $L_g e(z,t)>0$, in a sufficiently large open neighborhood of the sliding surface S, the control law, that locally forces the state trajectories to reach the sliding surface and thus acquires the possibility of "crossing" this surface, is given by

$$u(z,t)=\begin{cases}1 \text{ if } e(z,t)<0\\ 0 \text{ if } e(z,t)>0\end{cases},u=0.5(1-sign(e(z,t))) \tag{14}$$

Figure 4 shows block diagram of this proposed controller.

3. 2. 2. 1. Accessibility of The Sliding Surface The accessability condition which can be obtained from direct Lyapunove theorem is used to show the surface is attractive. When $u(z,t)=1$, according to Equation (2) $\dot{e}(z,t)=V_{pv}/L_1$ has positive value because input voltage of system is positive. When $u(z,t)=0$, the time derivative of $e(z,t)$ ($\dot{e}(z,t)=\frac{2V_{pv}-V_o}{L_1}<0 \Rightarrow V_o>2V_{pv}$) is a negative because the voltage gain G of the POSLL converter is $G=\frac{V_o}{V_{pv}}=\frac{2-D}{1-D}$, (where D is the duty cycle of the power switch), this shows the voltage gain G can changes from 2 to infinite theoretically.

3. 2. 2. 2. Proof of The Internal Stability Considering the state space equations and the designed control law, the system relative degree is one. So the system has internal dynamic and its stability should be investigated. This analysis can be done by zero dynamic study. According to Equations (2) and (10) the corresponding internal dynamic is given by:

$$\begin{aligned}\dot{v}_{pv}&=\left(\frac{i_{pv}-i_{L_1}}{c_1+c_{pv}}\right)\left(\frac{-2v_{pv}+v_o}{v_o-v_{pv}}\right)+\left(\frac{i_{pv}-i_{L_1}}{c_{pv}}\right)\left(\frac{v_{pv}}{v_o-v_{pv}}\right)\\ \dot{v}_O&=\frac{1}{c_2}\left(i_{L_1}-\frac{v_O}{R}-i_{L_1}\left(\frac{-2v_{pv}+v_o}{v_o-v_{pv}}\right)\right)\end{aligned} \tag{15}$$

To check the stability of the equilibrium point of (15), it is linearized around the equilibrium point $\bar{i}_{L_1}$. The corresponding Jacobian matrix J is given by:

$$J=\begin{pmatrix}J_{11} & J_{12}\\ J_{21} & J_{22}\end{pmatrix} \tag{16}$$

where

$$\begin{aligned}J_{11}&=\frac{\partial\dot{v}_{pv}}{\partial v_{pv}}=\frac{-I_o A\exp(v_{pv})}{v_o-v_{pv}}\left(\frac{v_o-v_{pv}}{c_1+c_{pv}}+\frac{v_{pv}}{c_{pv}}\right)+\left(\frac{i_{pv}-\bar{i}_L}{(v_o-v_{pv})^2}\right)v_o\left(\frac{1}{c_{pv}}-\frac{1}{c_1+c_{pv}}\right)\\ J_{12}&=\frac{\partial\dot{v}_{pv}}{\partial v_o}=\left(\frac{i_{pv}-\bar{i}_L}{(v_o-v_{pv})^2}\right)v_{pv}\left(\frac{-1}{c_{pv}}+\frac{1}{c_1+c_{pv}}\right)\\ J_{21}&=\frac{\partial\dot{v}_o}{\partial v_{pv}}=\frac{v_o}{(v_o-v_{pv})^2}\frac{\bar{i}_L}{c_2}\\ J_{22}&=\frac{\partial\dot{v}_o}{\partial v_o}=\frac{-v_o}{(v_o-v_{pv})^2}\frac{\bar{i}_L}{c_2}-\frac{1}{Rc_2}\end{aligned} \tag{17}$$

In (17), based on the PV generation modeling, $\dot{i}_{pv}$ is substituted by;

$$i_{pv}=I_{ph}-I_o(\exp(Av_{pv})-1) \tag{18}$$

where

$$\begin{aligned}A&=\frac{q}{N\gamma KT}\\ I_o&=I_{or}\left[\frac{T}{T_r}\right]^3\exp\left[\frac{qE_{GO}}{\gamma K}\left(\frac{1}{T_r}-\frac{1}{T}\right)\right]\\ I_{ph}&=\left[I_{scr}+K_I(T-T_r)\right]\frac{\lambda}{1000}\end{aligned} \tag{19}$$

where i_{pv} is the photocurrent (current generated by radiation); I_o is the cell reverse saturation current; I_{or} is the cell saturation current at T_r; I_{scr} is the short circuit current at 298.15K and $1Kw/m^2$; K_I is the short circuit current temperature coefficient at I_{scr}; λ is the solar radiation; E_{GO} is the band gap for silicon; γ is the ideality factor; T_r is the reference temperature; T is the ambient temperature input; q is the electron charge ($q=1.6\times10^{-19}$); K is the Boltzmann's constant ($K=1.3806505\times10^{-23}$).

With embedding steady state values in J_{11} of (14) one can obtain that the absolute value of the first term in J_{11} is larger than the absolute value of the second term in J_{11}, so J_{11} has negative value. J_{12} has positive value because $i_{pv}-\bar{i}_L>0$ and also $J_{21},J_{22}<0$. Since the following conditions are absolutely satisfied,

$$\begin{vmatrix}J_{11} & J_{12}\\ J_{21} & J_{22}\end{vmatrix}>0\ ,\ J_{11}<0 \tag{20}$$

So J is negative definite and the linearized system is strictly stable. Hence, based on the indirect Lyapunov stability theorem, the equilibrium point is asymptotically stable in the real non-linear system.

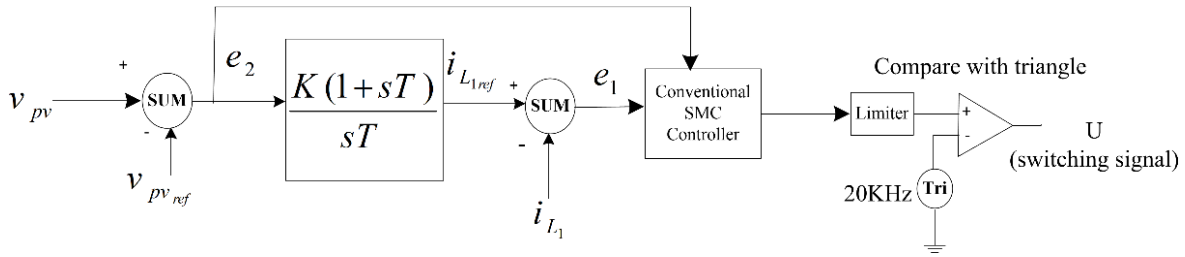

Figure 4. Schematic diagram of the proposed controller using conventional SMC

3. 3. SMC Controller Using Sign Function (SF-SMC)

The conventional SMC (CSMC) approach is employed to regulate the output voltage as the outer loop based on proportional–integral (PI) controller and an inner loop. Furthermore, the stability of the proposed CSMC is confirmed. CMSM is used for control of inductor current i_{L_1} and capacitor voltage v_{pv} as shown in Figure 4. The following sliding variable is defined for this purpose:

$$s_2(z,t) = K_1 e_1 + K_2 e_2 \tag{21}$$

where, K_1 and K_2 are positive constants; e_1 is the error between i_{L_1} and its reference, and e_2 is the error between v_{pv} and its reference which can be written as:

$$\begin{aligned} e_1 &= i_{L_{1_{ref}}} - i_{L_1} \\ e_2 &= v_{pv_{ref}} - v_{pv} \end{aligned} \tag{22}$$

where $i_{L_{1_{ref}}}$ is the inductor current reference that is obtained from comparison of the PV panel voltage and its reference using the PI controller. $v_{pv_{ref}}$ is the input capacitor voltage reference that can be obtained from an MPPT method.

Substituting (2) to the following equation the equivalent control law of POSLL converter can be obtained as Equation (25).

$$\dot{s}_2(z,t) = K_1 \dot{e}_1 + K_2 \dot{e}_2 = 0 \tag{23}$$

where

$$\dot{e}_1 = \dot{i}_{L_{1_{ref}}} - \dot{i}_{L_1}, \quad \dot{e}_2 = \dot{v}_{pv_{ref}} - \dot{v}_{pv}, \; u(z,t) = 1 - \frac{M}{N} \tag{24}$$

where

$$\begin{aligned} M &= K_1\left(\frac{v_{pv}}{L_1} - \dot{i}_{L_{1ref}}\right) + K_2\left(\dot{v}_{pv_{ref}} - \frac{(i_{pv} - i_{L_1})}{c_{pv}}\right) \\ N &= K_2\left(\frac{(i_{pv} - i_{L_1})}{c_{pv} + c_1} - \frac{(i_{pv} - i_{L_1})}{c_{pv}}\right) + K_1\left(\frac{v_o - v_{pv}}{L_1}\right) \end{aligned} \tag{25}$$

The designed control input is as follow:

$$u(z,t) = 1 - \frac{M}{N} - K_3 sign(S_2) - K_4 S_2 \tag{26}$$

where K_3 and K_4 are positive constants. $K_3 sign(S_2)$ is a discontinuous term to overcome some uncertainties in the system and $K_4 S_2$ is the modified term which increases the speed of convergence to the sliding surface. To implement the control law (25), the obtained u(z,t) should be compared to a saw tooth waveform and the result is used to command the converter switch. A simple similar control law can be used as follow,

$$u(z,t) = 0.5(1 - sign(e(z,t))) \tag{27}$$

which gives the switch command directly.

3. 3. 1. Proof of The Stability In this section the atractiveness of sliding surface $s_2 = 0$ using equivalent control law (25) is presented. The contol law (27) can be rewriten as

$$u(z,t) = \begin{cases} 1 \; if \;\; e(z,t) < 0 \\ 0 \; if \;\; e(z,t) > 0 \end{cases} \tag{28}$$

If $u(z,t) = 1$, $\dot{s}_2(z,t)$ is obtained as

$$\dot{s}_2(z,t) = K_1\left(\frac{-v_o}{L_1}\right) + K_2\left(\frac{i_{pv} - i_{L_1}}{c_{pv}}\right) \tag{29}$$

With selecting K_1 and K_2 somehow that the absolute of the first term of Equation (29) becomes larger than the second term, $\dot{s}_2(z,t) < 0$.

If $u(z) = 0$, $\dot{s}_2(z,t)$ is obtained as

$$\dot{s}_2(z,t) = K_1\left(\frac{v_o}{L_1}\right) + K_2\left(\frac{i_{pv} - i_{L_1}}{c_{pv} + c_1}\right) \tag{30}$$

Since $i_{pv} - i_{L_1} > 0$, $\dot{s}_2(z,t) > 0$.

According to the above discussion, the accesibility condition is satisficed and the sliding surface is atractive.

3. 3. 2. Proof of The Internal Stability The internal dynamic with conventional SMC method is expressed as:

$$\dot{v}_o = \frac{1}{c_2}(i_{L_1} - \frac{v_o}{R} - i_{L_1}u_{eq}) \quad (31)$$

where $u_{eq} = 1 - \frac{M}{N}$ that M and N are described in Equation (25). To verify the internal stability, (31) is linearized around the equilibrium point ($\bar{i}_{L_1}$, $\bar{v}_o$). Substituting (25) in Equations (31), (32) is obtained:

$$\frac{\partial \dot{v}_o}{\partial v_o} = \frac{1}{c_2}\left(\frac{-1}{R} + \frac{\frac{-K_1K_2\bar{i}_{L_1}(i_{pv}-\bar{i}_{L_1})}{(c_{pv}+c_1)L} + \frac{K_1^2\bar{i}_{L_1}\bar{v}_{pv}}{L^2}}{(K_1\frac{v_{pv}-v_o}{L} + K_2\frac{i_{pv}-\bar{i}_{L_1}}{c_{pv}} + \frac{K_2(-i_{pv}+\bar{i}_{L_1})}{(c_{pv}+c_1)})^2}\right) \quad (32)$$

In Equation (32), if $K_2 > K_1$ is chosen large enough, then $\frac{\partial \dot{v}_o}{\partial v_o} < 0$; thus the internal dynamic of conventional SMC method will be stable.

4. SIMULATION AND EXPERIMENTAL RESULTS

A DC–DC POSLL converter as depicted in Figure 2 with nominal parameters given in Table 1 is considered.

In order to show the effectiveness of the proposed controllers, simulation and practical results are obtained in three distinct tests. The PV module specifications are listed in Table 2. The step time of the simulation is $1\mu s$. The switching frequency is 20 KHz. The experimental results have been obtained by a laboratory prototype depicted in Figure 5.

4. 1. PI Controller Results According to Figure 3, two control loops are simulated and implemented in practical using the Discovery board. The outer loop PI controller coefficients set to $K_2 = 1$ and $T_2 = 0.1$. The inner loop PI controller coefficients are $K_1 = 2$ and $T_1 = 0.1$. In simulation results depicted in Figures 6(a) and 6(b), the converter input reference voltage is stepped down and up from V_{ref} =8 to 4 V at t = 0.6 s and from 4 to 8 V at t=2.6 s respectively. In practical test, the same input reference voltage is used. The practical obtained results are shown in Figure 6(c). It can be seen that the input voltage follows the reference value and the experimental results confirm the simulation results. It is worthwhile to note the converter capacitors are large (1mF) and they decrease the speed of the responses.

TABLE 1. Characteristic of system parameters for both the hardware and the simulation configurations.

Parameter	Description	Value
C_{pv}	Input Capacitor of system	100μF
C_1	Boost Capacitor of converter	1mF
C_2	Input Capacitor of converter	1mF
L_1	Inductor o converter	100μH
R	Load resistance	50Ω

TABLE 2. Characteristic of system parameters

Description	Value
Number of cell	36
Maximum power	5 W
Voltage at maximum power	18.5 V
Open circuit voltage	22.56 V
Reference cell temperature	25 °C
Standard light intensity at 25 °C	1000w/m^2
Current at maximum power	0.25
Short circuit current	0.3A

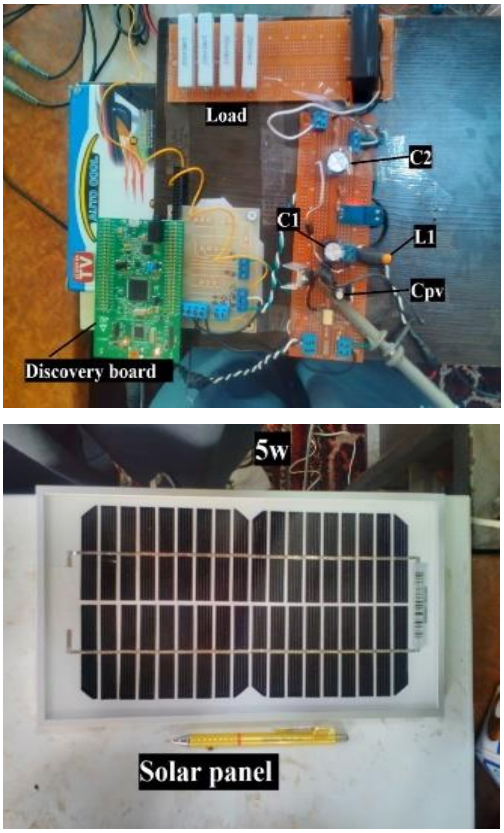

Figure 5. Experimental setup

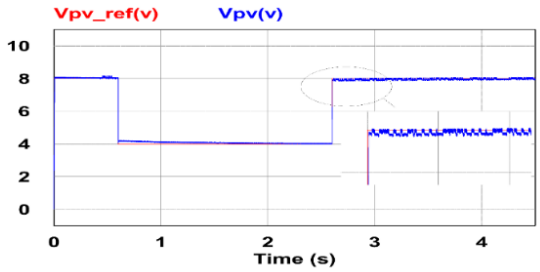

(a)

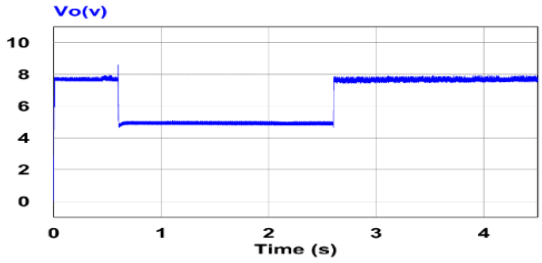

(b)

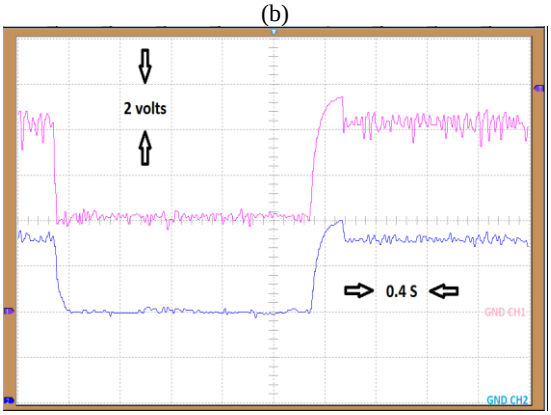

(c)

Figure 6. Simulation and experimental results with step change of input voltage reference in PI controller. Simulation results: (a) input voltage and its reference, (b) output voltage, Experimental results: (c) input voltage (CH1), output voltage (CH2).

4. 2. SF- SMC Controller Results In Figure 7 the DC-DC POSLL converter is controlled using SFC method in order to achieve to reference value of PV panel regarding to (10). Like before, the converter input reference voltage is stepped down from $v_{pv_{ref}}$ = 8 to 6 V at t = 0.6 s and comes back to 8 V at t=2.6 s in obtaining simulation results. The same reference input voltage is used in experimental test. Figures 8 (a) and (b) show simulation results and Figure 8 (c) shows experimental results. Using one PI controller, tuning the controller is easier. Parameters of PI controller are set by try and error to $K = 0.1 \& T = 1$.

4. 3. Conventional SMC Results The conventional SMC block diagram is shown in Figure 7. The composition of linear controller (PI) and nonlinear controller is used for input voltage control of PV system. The parameters of control law (26) are selected by try and error to achieve the best response and stability. The values of K_1 to K_4 and $K \& T$ of PI controller are listed in Table 3. Considering the same condition as the two previous controller tests, the simulation and practical results are shown in Figure 8.

4. 4. Comparison and Discussion The three controllers proposed to control the input voltage of the PV system are compared and discussed in this section. Using each of these controllers, the reference input voltage is followed; however, the conventional SMC controller has a better performance. As shown in Figure 8(a), there is less error between PV voltage and its reference than SF-SMC controller and PI controller. Also, reference tracking in SF-SMC controller (Figure 9(a)) is better than PI controller (Figure 7 (a)). The simulation results show that the delivered input voltage in PI controller comes with distortion, while the quality of input voltage in SF-SMC controller is acceptable, the practical results also confirm it.

Output voltages of the stand-alone PV system are brought in Figures 7(b), 8(b) and 9(b) for PI, SMC and SF- SMC controller, respectively. The output voltage of system changes with the change in the input voltage. Comparing output voltages of the proposed system with the presented controllers, shows that the output voltage of the system with SFC controller has more chattering

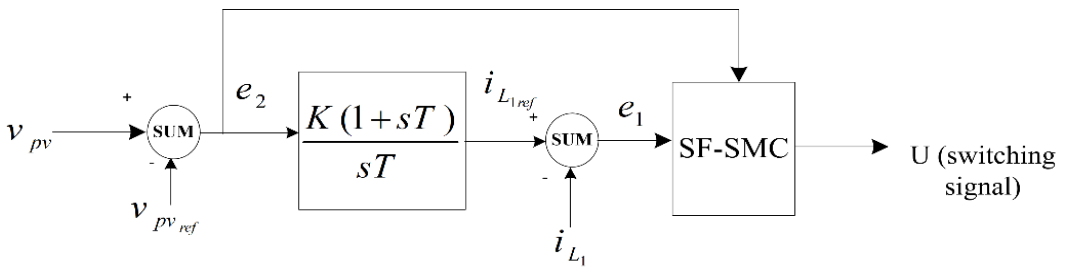

Figure 7. Schematic diagram of the proposed controller using SF-SMC

TABLE 3. Constance of controller for CSMC

Constance	Value
K_1	1000
K_2	1000
K_3	500
K_4	500
K	1
T	0.5

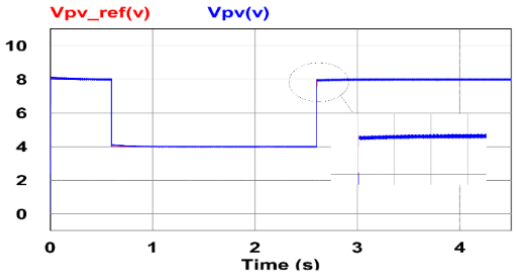

(a)

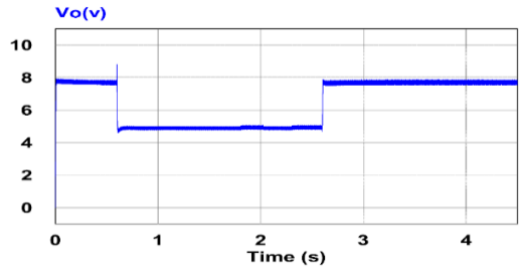

(b)

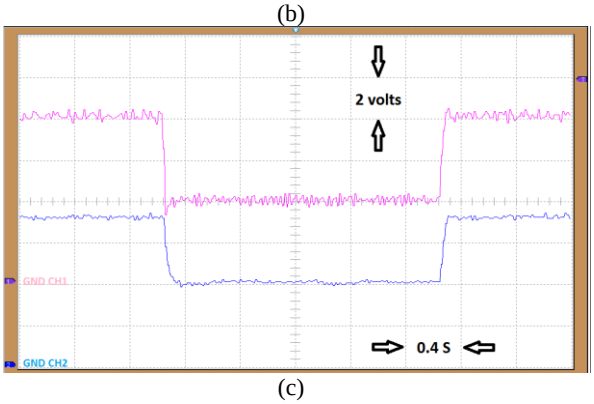

(c)

Figure 8. Simulation and experimental results with step change of input voltage reference in SMC. Simulation results: (a) input voltage and its reference. (b) output voltage. Experimental results: (c). input voltage (CH1), output voltage (CH2).

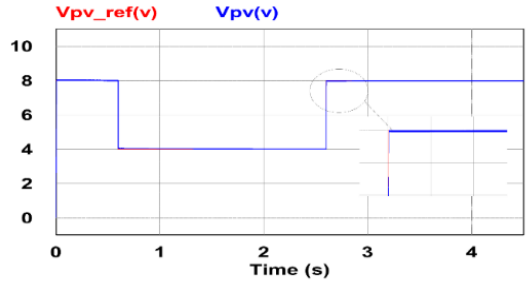

(a)

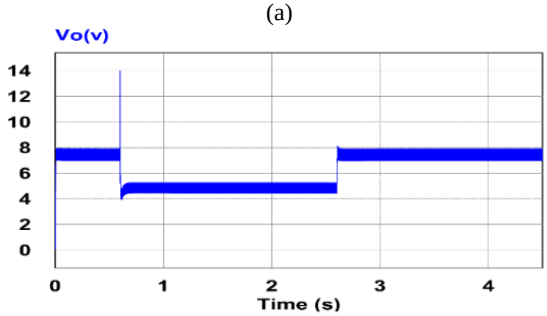

(b)

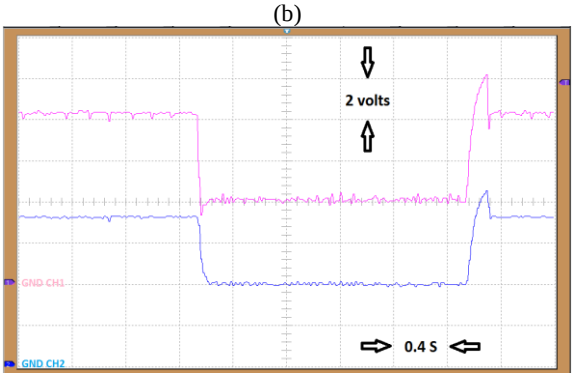

(c)

Figure 9. Simulation and experimental results with step change of input voltage reference in SF-SMC. Simulation results: (a) input voltage and its reference. (b) output voltage. Experimental results: (c). input voltage (CH1), output voltage (CH2).

than others. In experimental results (Figures 9(c) and 8(c)) the output voltage of system with SF-SMC controller and the conventional SMC are almost the same and has a better quality than the results obtained with PI control. The maximum overshoot precents in input voltage using PI control, SF-SMC and conventional SMC are about %33, %50, 0 respectively, and the correspondent rise times are about 72, 64 and 72 ms respectively. Table 4 presents a summary of comparison of the performance and implementation of the proposed controllers.

TABLE 4. Performance comparison of the proposed controllers.

Description	Using PI controller	Using SF-SMC	Using CSMC
Reference tracking	Not bad	Good	Very good
Quality of input voltage	Poor	Very good	Very good
Practical implementation	Simple	Relatively simple	Difficult
operating point area	Wide	Very Wide	Very Wide
Stability	Low	High	High
Quality of output voltage	Good	Very good	Very good

5. CONCLUSION

Two sliding mode controllers suitable for regulating the DC bus voltage of a stand-alone PV system including a POSLL converter is presented and compared. The stability and accessibility of the proposed nonlinear controls are investigated with the theoretical analysis, the extended simulation, and experimental results. The proposed system takes advantages of a DC-DC POSLL converter such as; high voltage gain, smoother output voltage and lower inductance current. It has been shown that the use of a nonlinear controller in indirect control of the panel voltage results in more efficiency and better performance.

6. REFERENCES

1. Heidari, H. and Tarafdar Hagh, M., "Optimal reconfiguration of solar photovoltaic arrays using a fast parallelized particle swarm optimization in confront of partial shading", ***International Journal of Engineering, Transaction B: Applications***, Vol. 32, No. 8, (2019), 1177-1185.
2. Dhass, A., Natarajan, E. and Lakshmi, P., "An investigation of temperature effects on solar photovoltaic cells and modules", ***International Journal of Engineering, Transaction B: Applications***, Vol. 27, No. 11, (2014), 1713-1722.
3. Mellit, A., Benghanem, M. and Kalogirou, S.A., "Modeling and simulation of a stand-alone photovoltaic system using an adaptive artificial neural network: Proposition for a new sizing procedure", ***Renewable Energy***, Vol. 32, No. 2, (2007), 285-313.
4. Mahdavi, M., Shahriari-kahkeshi, M. and Abjadi, N.R., "An adaptive estimator-based sliding mode control scheme for uncertain poesll converter", ***IEEE Transactions on Aerospace and Electronic Systems***, Vol. 55, No. 6, (2019), 3551-3560.
5. Nasiri, H., Goudarzian, A. and Abjadi, N.R., "Design and implementation of a constant frequency sliding mode controller for a luo converter", ***International Journal of Engineering, Transaction B: Applications***, Vol. 29, No. 2, (2016), 202-210.
6. Miao, Z. and Fang Lin, L., "Analysis of positive output super-lift converter in discontinuous conduction mode", In 2004 International Conference on Power System Technology, 2004. PowerCon 2004. Vol. 1, (2004), 828-833
7. Jiao, Y., Luo, F.L. and Zhu, M., "Generalised modelling and sliding mode control for n-cell cascade super-lift dc-dc converters", ***IET Power Electronics***, Vol. 4, No. 5, (2011), 532-540.
8. He, Y. and Luo, F.L., "Analysis of luo converters with voltage-lift circuit", ***IEE Proceedings - Electric Power Applications***, Vol. 152, No. 5, (2005), 1239-1252.
9. Konstantopoulos, G.C. and Alexandridis, A.T., "Non-linear voltage regulator design for dc/dc boost converters used in photovoltaic applications: Analysis and experimental results", ***IET Renewable Power Generation***, Vol. 7, No. 3, (2013), 296-308.
10. Chaibi, Y., Salhi, M. and El-Jouni, A., "Sliding mode controllers for standalone pv systems: Modeling and approach of control", ***International Journal of Photoenergy***, Vol. 2019, (2019).
11. Kamran, A., Laiq, K., Qudrat, K., Shafaat, U., Saghir, A., Sidra, M., Fazal Wahab, K. and Naghmash, "Robust integral backstepping based nonlinear mppt control for a pv system", ***Energies***, Vol. 12, No. 16, (2019), 1-20.
12. Miqoi, S., Ougli, A.E. and Tidhaf, B., "Adaptive fuzzy sliding mode based mppt controller for a photovoltaic water pumping system", ***International Journal of Power Electronics and Drive System (IJPEDS)***, Vol. 10, No. 1, (2019), 414-422.
13. Assam, B., Messalti, S. and Harrag, A., "New improved hybrid mppt based on backstepping-sliding mode for pv system", ***Journal Européen des Systèmes Automatisés***, Vol. 52, No. 3, (2019), 317-323.

Nonlinear Control for Positive Output Super Lift Luo Converter in Stand Alone Photovoltaic System

S. A. A Fallahzadeh[a], N. R Abjadi[a], A. Kargar[a], F. Blaabjerg[b]

[a] *Faculty of Engineering, Shahrekord University, Shahrekord, Iran*
[b] *Department of Energy Technology, Aalborg University, Aalborg, Denmark*

P A P E R I N F O

Paper history:
Received 27 September 2019
Received in revised form 27 October 2019
Accepted 16 Januray 2020

Keywords:
Photovoltaic
Sliding Mode Controller
Stand Alone
Super Lift Luo converter

چکیده

در این مقاله یک سیستم فتوولتائیک منفصل از شبکه بر پایه مبدل *POSLL DC-DC* ارائه شده است. یک کنترل کننده مد لغزشی مرسوم، یک کنترل کننده مد لغزشی با استفاده از تابع علامت و یک کنترل کننده خطی تناسبی – انتگرالی برای کنترل ولتاژ پنل و جریان سلف مبدل استفاده شده است و این روش‌ها با یکدیگر مقایسه شده‌اند. مبدل *POSLL* یک مبدل *DC-DC* است که نسبت به مبدلهای *DC-DC* مرسوم دیگر بهره ولتاژ بالاتری دارد و از تنظیم ولتاژ خوب و ساختار ساده‌ای برخوردار است. پایداری این کنترل کننده‌ها نیز به طور وسیعی بررسی شده است. دینامیک داخلی سیستمهای حلقه بسته کنترلی پیشنهادی نیز بررسی شدند. پیاده‌سازی عملی و سخت‌افزاری با استفاده از بورد ارزان قیمت دیسکاوری زمان حقیقی اجرا شده است. نتایج شبیه سازی و عملی، قابلیت و صحت کارآیی کنترل کننده‌های طراحی شده را بر روی یک سیستم فتوولتائیک منفصل از شبکه ارائه می‌دهد.

***doi**: 10.5829/ije.2020.33.02b.08*